Tunnelling and Underground Space Technology 85 (2019) 84–91

Contents lists available at ScienceDirect

Tunnelling and Underground Space Technology

journal homepage: www.elsevier.com/locate/tust

Simulating three dimensional hydraulic fracture propagation using displacement correlation method

Nithin Manohar Rayudu[a], Xuhai Tang[b], Gaurav Singh[c,*]

[a] Department of Mechanical Engineering, BITS, Pilani – Goa Campus, Goa 403726, India
[b] School of Civil Engineering, Wuhan University, Wuhan 430072, China
[c] Department of Applied Mechanics, Indian Institute of Technology Delhi, New Delhi 110016, India

ARTICLE INFO

Keywords:
Hydraulic fracture
Orientation
TOUGH-FEMM
Displacement Correlation

ABSTRACT

The TOUGH-FEMM simulator is used to investigate the interaction of multiple simultaneous hydraulic fractures. In TOUGH-FEMM simulator, rock deformation is modeled using the hybrid Finite Element-Meshfree Method (FEMM) and fluid flow is simulated through the Transport Of Unsaturated Groundwater and Heat (TOUGH2) simulator. The stress intensity factors are calculated by using the Displacement Correlation Method (DCM). The equivalent mode I stress intensity factor is used for determining fracture propagation criterion and direction. Successfully creating multiple hydraulic fractures in horizontal wells is critical for unconventional gas production economically. These previous works focussed on the propagation of fractures which are parallel initially. However, because of inevitable error in practical engineering and natural flaws in rock, the initial fractures might be inclined. The overall objective of the current work is to study the influence of initial fracture orientation on the simultaneous hydraulic fracturing of a horizontal well. The results of the present work show that initial fracture orientation has significant effect on the fracture propagation direction and final fracture contour. Different fracture contours will result in distinct fracture network, which will greatly affect the reservoir permeability.

1. Introduction

Hydraulic fracture is used for the extraction of natural oil and gas from shale rock. In this technique, large amount of fluids and proppants are pumped into shale rock for natural gas extraction by creating fractures and increasing the permeability of the shale rock (Yang et al., 2018; Lu et al., 2015; Hou et al., 2016). Presently, Canada, United States and China are the largest shale gas producing countries. In this process, a well is drilled to around 2500 m below the earth's surface. Thereafter, for maximum gas output, horizontal drilling is done for hundreds of meters. After horizontal drilling, perforation guns punch holes through the casing to form initial fractures (Osiptsov, 2017). Later, pressurized fluid is pumped in order to generate fracture networks which enhances the permeability of the reservoirs (Fisher and Warpinski, 2012). Hydraulic fracturing is also widely used in mining (He et al., 2016) where it is used for preconditioning of rock (artificial weakening of the orebody) so that easy extraction of the ore is possible. Hydraulic fracturing is also used for improving the coal seam permeability (Zhai et al., 2012) and for initiating caving process (Katsaga et al., 2015). The hydraulic fracture lengths in mining are generally small compared to that in shale gas extraction process (He et al., 2016).

Understanding the fracture propagation behavior is vital for optimizing the hydraulic fracture design. There are many factors such as fracture length (Su et al., 2015), orientation (Castonguay et al., 2013), and viscosity of the fluid (Zhou and Burbey, 2014), which will influence the fracture propagation behavior. Initial fracture orientation is one of the important factors which will effect the stress distribution at the vicinity of the fracture, which results in changing fracture propagation direction (Mei et al., 2011). The focus of the present work is to study the effect of initial fracture orientation on the fracture propagation behavior.

Many researchers have been working on the study of hydraulic fracture for many decades. In early years, efforts were focused on fractures with straight or penny-shaped geometry (Christianovich and Zheltov, 1955; Perkins and Kern, 1961). Two commonly used techniques for investigating hydraulic fracturing are physical experiments (Yan et al., 2016; Ishida, 2001; Zhao et al., 2015) and numerical analysis (Yang et al., 2018; Yang et al., 2016). Physical experiments give accurate results but conducting actual scale and fabricating complex fracture network is often difficult. Numerical analysis partly overcomes

* Corresponding author.
E-mail address: gsingh@am.iitd.ac.in (G. Singh).

https://doi.org/10.1016/j.tust.2018.11.010
Received 31 March 2018; Received in revised form 5 October 2018; Accepted 17 November 2018
Available online 07 December 2018
0886-7798/

the above problem as it is capable of simulating complex loading and geometries.

FEM is a well known method for simulating fracture propagation in geomechanics (Castelletto et al., 2017) because of its ability to handle complex geometry and loading conditions. In FEM, the fracture will propagate along element boundary and will require re-meshing around fracture tip in every step of the growth (Paluszny and Zimmerman, 2013). Based on the partition of unity method (Melenk and Babuška, 1996), a large number of numerical methods have been developed in which fracture propagation can be simulated without re-meshing, including Generalized FEM (GFEM) (Gupta and Duarte, 2016), eXtended FEM (XFEM) (Moës et al., 1999; Sukumar et al., 2000), enriched numerical manifold method (Yang et al., 2018), polygonal FEM (Tang et al., 2009) and Meshfree methods (Belytschko et al., 1994). Gupta and Duarte (2016) presented a methodology for three dimensional fracture propagation using G/XFEM. In order to take the advantage of both methodologies (FEM and meshfree), hybrid FE-Meshfree Methods (FEMM) have been developed (Rajendran and Zhang, 2007).

The fractures in hydraulic fracture propagate due to high fluid pressure. A coupling between the fluid and solid mechanics is thus necessary. In this paper, the TOUGH-FEMM simulator is used to investigate the interacting of two simultaneous hydraulic fractures. In this TOUGH-FEMM simulator, rock deformation is modeled using FEMM and fluid flow is simulated through the Transport Of Unsaturated Groundwater and Heat (TOUGH2) simulator. The fracture propagation criterion and direction is based on the stress intensity factors (SIF) around the crack tip. Displacement Correlation Method (DCM) (Nejati et al., 2015; Minnebo et al., 2010) is a direct method based on displacement for calculating the SIF at the fracture tip. In DCM, the domain around fracture tip is not needed for the calculation of SIFs. TOUGH2 is a well established code for analyzing flow and heat transfer in geological media (Pruess et al., 1999; Rinaldi and Nespoli, 2017; Jung et al., 2017; Rinaldi and Rutqvist, 2017). Various TOUGH2 based simulators have been developed till date for simulating geomechanics with fluid flow. Rutqvist (2011) simulated coupled fluid heat transfer with geomechanics using TOUGH-FLAC simulator. Kim and Moridis (2013) modeled a FEM based coupled fluid geomechanics simulator using TOUGH. As of present, there are more than 15 different TOUGH2 based simulators developed by different researchers (Rutqvist, 2017).

Successfully creating multiple hydraulic fractures in horizontal wells is critical for unconventional gas production economically. Optimizing the stimulation of these wells will require models that can account for the simultaneous propagation of multiple, potentially nonplanar, fractures. Many references (Wu and Olson, 2013; Wu and Olson, 2015; Wu et al., 2012) has discussed the influence of in situ stress and fracture length on the simultaneous hydraulic fractures. These previous work focus on the propagation of fractures which are in parallel initially. However, because of inevitable error in practical engineering and natural flaws in rock, the initial fractures might be inclined.

The overall objective of the current work is to study the influence of initial fracture orientation on the simultaneous hydraulic fracturing of a horizontal well. The FEMM-TOUGH2 simulator Tang et al. is used for simulating hydraulic fracture propagation and DCM is used for calculating the SIFs. The outline of this paper is as following: Section 2 explains the fundamentals of FEMM, Section 3 provides the description for linking FEMM with TOUGH2 and Section 4 describes the process of fracture updation. Finally, Section 5 is dedicated to validation of the method adopted here followed by Section 6 in which the effect of initial fracture orientation on propagation has been studied.

2. Finite Element-Meshfree Method (FEMM)

In this section, the hybrid Finite Element-Meshfree Method (FEMM) (Liu et al., 2018; Yang et al., 2017) is introduced, which is then used to model the rock deformation. Consider a bounded domain $\prod$ in three

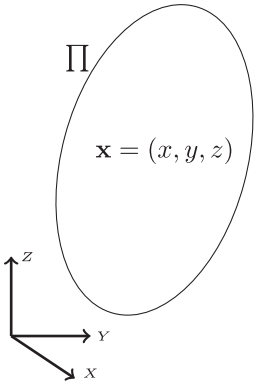

Fig. 1. Bounded domain.

dimensions as shown in Fig. 1. By the principle of partition of unity element method (PUM) (Melenk and Babuška, 1996), for a set of non-negative weight functions ($\omega_1(\mathbf{x})$, $\omega_2(\mathbf{x})$, $\omega_3(\mathbf{x})$, …$\omega_N(\mathbf{x})$), whose sum is equal to unity as

$$\sum_{i=1}^{N} \omega_i(\mathbf{x}) = 1 \tag{1}$$

where $\mathbf{x} = (x, y, z)$ is a point inside the domain and N is the total number of nodes, the approximation in domain $\prod$ can be defined as Yang et al. (2014)

$$u^h(\mathbf{x}) = \sum_{i=1}^{N} \omega_i(\mathbf{x}) u_i(\mathbf{x}) \tag{2}$$

where $u_i(\mathbf{x})$ is the approximated value at the node i.

In the present work, the domain is discretized with tetrahedral elements. A generalized tetrahedral element $\boldsymbol{\Omega}$ with vertices $P = (P_1, P_2, P_3, P_4)$, which is passed by a planar fracture, is shown in Fig. 2. At an arbitrary point $\mathbf{x} = (x, y, z)$, by the principle of partition of unity (Melenk and Babuška, 1996) for non-negative weight functions (ω_1, ω_2, ω_3, ω_4) in a generalized domain, the sum of weight functions is equal to unity

$$\omega_1(\mathbf{x}) + \omega_2(\mathbf{x}) + \omega_3(\mathbf{x}) + \omega_4(\mathbf{x}) = 1 \tag{3}$$

Fig. 3 shows different kinds of elements i.e. fracture elements, bridge elements and ordinary FE elements. Elements intersected by fracture are called fracture elements. Elements adjacent to fracture elements are called bridge elements and remaining are ordinary FE elements. Two kinds of nodes are used, ordinary finite element (FE)

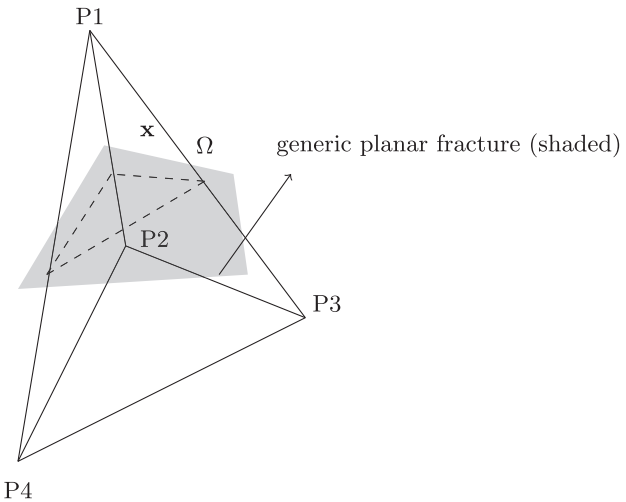

Fig. 2. Tetrahedral element cut by a generic planar fracture.

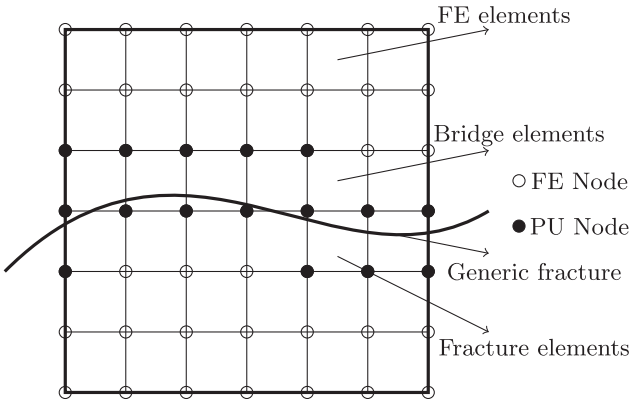

Fig. 3. Different element and node type.

nodes and partition of unity (PU) nodes. All nodes within fracture elements are PU nodes and all the remaining nodes are ordinary FE nodes. The global approximation of elements in domain Ω is written as

$$u^h(\mathbf{x}) = \sum_{i=1}^{4} \omega_i(\mathbf{x}) u_i(\mathbf{x}) \tag{4}$$

where $u_i(\mathbf{x})$ is the local approximation associated with node i.

Weight functions of FE nodes is taken as 1 and the least square method is used for constructing local approximation for PU nodes. Fig. 4 shows the node patch of node i defined as the union of elements that share the node i along with the nomenclature of node types. The element support is given from the union of four node patches

$$\hat{\Omega} = \bigcup_{i=1}^{4} \Omega_i \tag{5}$$

For fracture elements, the discontinuous displacement field across the fracture surface needs to be modeled accurately. The starting index set of nodes ψ_Ω is related to an element domain with a visibility criterion. We define the visibility zones $\psi_\Omega^{vis} \in \psi_\Omega$ as

$$\psi_\Omega^{vis} = \{\mathbf{x}_i \in \psi_\Omega \,|\, [\mathbf{x} - \mathbf{x}_i] \cap \text{fracture surface} = \phi\} \tag{6}$$

where $\mathbf{x}_i$ is the coordinate of node i. For constructing discontinuous approximation along fracture surface, Shepard's Formula (Lancaster and Salkauskas, 1986) is used. The weight functions are given, in terms of sub-weight functions $\phi = \{\phi_1', \phi_2'', \phi_3'', \phi_4''\}$ as

$$\omega_i(\mathbf{x}) = \frac{\phi_i'(\mathbf{x})}{\phi_1'(\mathbf{x}) + \phi_2'(\mathbf{x}) + \phi_3'(\mathbf{x}) + \phi_4'(\mathbf{x})} \tag{7}$$

$$\phi_i'(\mathbf{x}) = \begin{cases} \phi_i(\mathbf{x}) & \text{if } x \in \Psi^{vis} \\ 0 & \text{otherwise} \end{cases} \tag{8}$$

where $\phi_i(\mathbf{x})$ is constructed from tetrahedron FE shape functions and can be given as

$$\phi_1(\mathbf{x}) = \frac{\text{vol}(p(\mathbf{x})p_2p_3p_4)}{\text{vol}(p_1p_2p_3p_4)} \quad \phi_2(\mathbf{x}) = \frac{\text{vol}(p(\mathbf{x})p_3p_4p_1)}{\text{vol}(p_1p_2p_3p_4)}$$
$$\phi_3(\mathbf{x}) = \frac{\text{vol}(p(\mathbf{x})p_4p_1p_2)}{\text{vol}(p_1p_2p_3p_4)} \quad \phi_4(\mathbf{x}) = \frac{\text{vol}(p(\mathbf{x})p_1p_2p_3)}{\text{vol}(p_1p_2p_3p_4)} \tag{9}$$

where vol(p_1, p_2, p_3, p_4) is the volume of tetrahedron,

vol $(p(\mathbf{x}), p_i, p_j, p_k)$ is the volume of the tetrahedron formed by an arbitrary point $\mathbf{x}$ and vertices of the tetrahedron p_i, p_j and p_k.

For FE elements, the local approximation is taken as unity and weight functions are chosen as standard FE shape functions of the tetrahedron elements. The shape functions can be given as

$$N_1(\mathbf{x}) = \frac{\text{vol}(p(\mathbf{x})p_2p_3p_4)}{\text{vol}(p_1p_2p_3p_4)} \quad N_2(\mathbf{x}) = \frac{\text{vol}(p(\mathbf{x})p_3p_4p_1)}{\text{vol}(p_1p_2p_3p_4)}$$
$$N_3(\mathbf{x}) = \frac{\text{vol}(p(\mathbf{x})p_4p_1p_2)}{\text{vol}(p_1p_2p_3p_4)} \quad N_4(\mathbf{x}) = \frac{\text{vol}(p(\mathbf{x})p_1p_2p_3)}{\text{vol}(p_1p_2p_3p_4)} \tag{10}$$

The formulae for calculating weight functions of bridge elements is equivalent to standard FE formula, which can be given as

$$\omega_1(\mathbf{x}) = \frac{\text{vol}(p(\mathbf{x})p_2p_3p_4)}{\text{vol}(p_1p_2p_3p_4)} \quad \omega_2(\mathbf{x}) = \frac{\text{vol}(p(\mathbf{x})p_3p_4p_1)}{\text{vol}(p_1p_2p_3p_4)}$$
$$\omega_3(\mathbf{x}) = \frac{\text{vol}(p(\mathbf{x})p_4p_1p_2)}{\text{vol}(p_1p_2p_3p_4)} \quad \omega_4(\mathbf{x}) = \frac{\text{vol}(p(\mathbf{x})p_1p_2p_3)}{\text{vol}(p_1p_2p_3p_4)} \tag{11}$$

A brief introduction to FEMM has thus been given. In the next section, the TOUGH-FEMM simulator is described in some detail.

3. TOUGH and FEMM coupling

Numerical simulation of hydraulic fracturing consists of three processes:

- Fluid flow in the fracture surface and surrounding porous rock
- Fracture propagation in the rock
- Induced deformation in rock due to fluid flow on the fracture surface

For modeling hydraulic fracturing accurately, two-way coupling is required between hydraulic and mechanical processes (Rutqvist and Stephansson, 2003). In the current work, FEMM-TOUGH2 simulator developed in Ref. Tang et al. is applied to simulate hydraulic fracturing, which combines the solid solver (FEMM) and the fluid solver (TOUGH2) as shown in Fig. 5. FEMM solver is used for calculating the rock deformation and TOUGH2 solver (Pruess et al., 1999) is used for calculating fluid pressure on the fracture surface. The present work is focussed towards implementation of the DCM in FEMM where fracture surface is discretized with triangular elements. In the next section, fracture propagation criteria and fracture updation are discussed briefly.

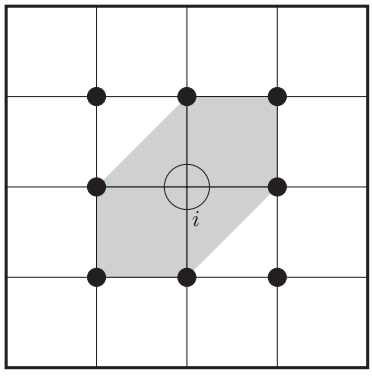

Fig. 4. Node patch for central node i.

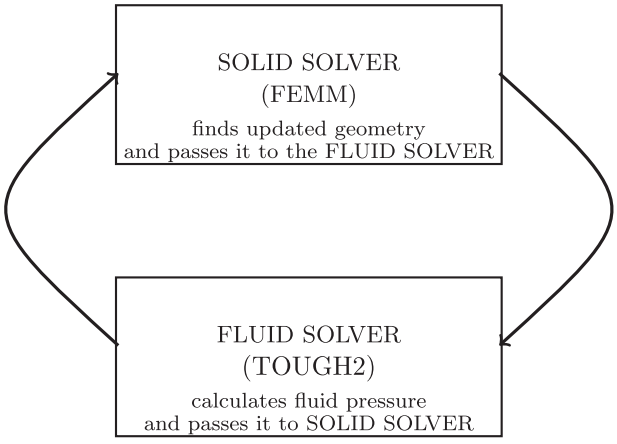

Fig. 5. Two way fluid-solid coupling.

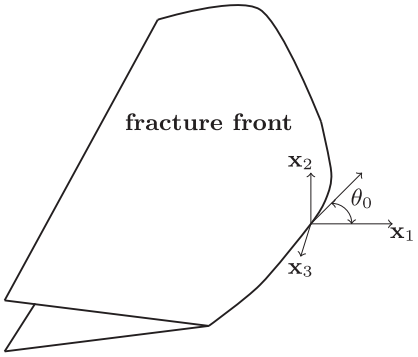

Fig. 6. Fracture propagation direction (θ_o) in local coordinate system ($\mathbf{x_1}$,$\mathbf{x_2}$, $\mathbf{x_3}$).

4. Fracture propagation

Even though multiple fracture propagation criteria like minimum strain energy density (Sih, 1974) and maximum strain energy release rate (Strifors, 1974) exist, the direct approach (Nejati et al., 2015) on displacements is used, which is attractive due to the fact that the displacement fields are the most accurate fields obtained from FEMM solutions. Locally, the 3D field solution can be approximated by the 2D plane strain fields (Nakamura and Parks, 1988; Nakamura and Parks, 1989). The stress field near any point on the fracture front is sequentially considered to be in the form of this singular field in the plane strain condition (Anderson, 2005). This criteria is mathematically represented as

$$K_I \sin(\theta_o) + K_{II}(3\cos(\theta_o) - 1) = 0 \tag{12}$$

where K_I and K_{II} are mode *I* and mode *II* stress intensity factors, θ_o is the fracture propagation direction as shown in Fig. 6. The simplified form of the above equation can be given as

$$\tan\left(\frac{\theta_o}{2}\right) = \frac{1}{4}\left(\frac{K_I}{K_{II}} - sgn(K_{II})\sqrt{\left(\frac{K_I}{K_{II}}\right)^2 + 8}\right), \quad -\pi \leqslant \theta_o \leqslant \pi \tag{13}$$

where *sgn* is the signum function. Mode *I* equivalent stress intensity factor (Castonguay et al., 2013) is the combination of mode *I* and mode *II* stress intensity factors. The stress intensity factors K_I and K_{II} can be calculated from the (Nejati et al., 2015) to write equivalent mode *I* stress intensity factor as

$$K_{I_{eq}} = K_I \cos^3\left(\frac{\theta_o}{2}\right) - \frac{3}{2}K_{II}\cos\left(\frac{\theta_o}{2}\right)\sin(\theta_o) \tag{14}$$

The fracture propagation will occur when $K_{I_{eq}}$ exceeds critical stress intensity factor, i.e.

$$K_{I_{eq}} \geqslant K_{critical} \tag{15}$$

The equivalent SIF $K_{I_{eq}}$ may be interpreted as a unified fracture criterion in the presence of mixed-mode conditions. This is similar to many of the failure criteria used to predict the onset of yielding in multi-axial loading conditions.

When fracture propagation criterion is met [Eq. (15)], then the propagation vector is used for determining new fracture tip nodes. New nodes and elements for fracture are generated from the old as shown in Fig. 7. Further details of the geometric evolution can be found in an earlier literature (Paluszny and Zimmerman, 2013).

In the next section, the proposed algorithm is validated with the existing literature.

5. Validation

Testing the robustness and accuracy of the proposed method for studying the effect of initial fracture orientation in hydraulic fracturing,

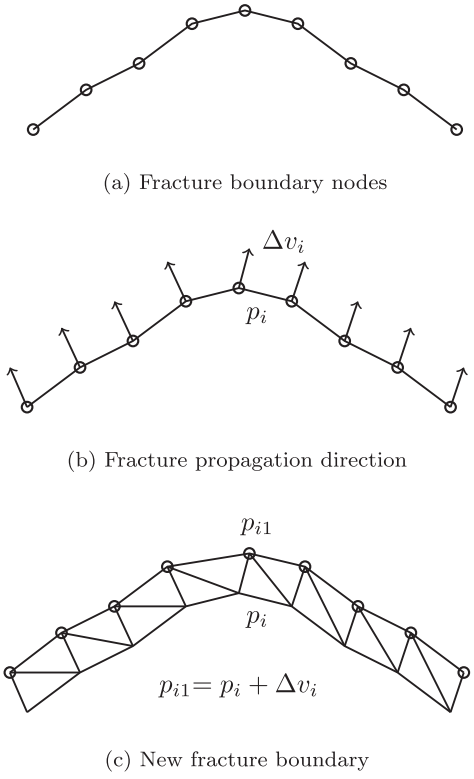

Fig. 7. Fracture updation process.

some numerical examples are simulated in this section and are validated with the existing literature. Multiple hydraulic fracture propagation and interactions are illustrated here. In the following examples, hydraulic fractures up to three are considered, but the proposed algorithm can simulate more than three hydraulic fractures. Here, the fluid flow rate is considered as constant for simplicity and the fracture growth will initiate simultaneously. In the proposed algorithm, the fracture growth up to intersection is considered while ignoring the fracture crossing each other. These examples show that multiple simultaneous fracture propagation has a significant influence on the final fracture contour.

5.1. Two parallel fractures

In this example, a horizontal wellbore intersected by two perpendicular circular fractures is simulated for constant flow rate (as shown in Fig. 8). The boundaries of the rock sample are very far from the wellbore to avoid any boundary effects. The material properties, dimensions, and flow input parameters considered are given in Table 1 (after Castonguay et al., 2013).

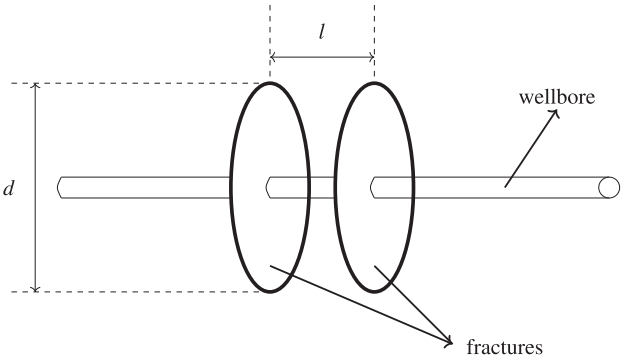

Fig. 8. A wellbore intersected by two parallel fractures.

Table 1
Input parameters for two parallel fractures.

Input parameters	Value
Flow rate (kg/s)	10
Poisson's ratio	0.25
Elastic modulus (GPa)	30
Rock porosity	0.1
Permeability (m^2/s)	10^{-12}
Diameter of the fractures (m), d	5
Distance between fracture (m), l	5

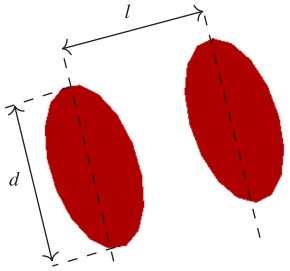

Fig. 9. Initial geometry of two parallel fractures without wellbore.

After fluid injection, the fractures start propagating radially and each fracture is influencing the other fracture due to stress shadow effect (i.e. changing stress field in the vicinity of one fracture due to the fracture opening of the other) (He et al., 2017; Taleghani et al., 2018; Shimizu et al., 2018). Due to this stress shadow effect, the fractures were propagating away from each other and produced a bowl-like contour (Wu and Olson, 2013). The initial fracture geometry is shown in Fig. 9. It had been analytically shown earlier (sans the term "stress shadow") using stress fields that two cracks growing towards each other avoid a head-on confrontation before coalescence (Melin, 1983).

The simulation is run as long as the fractures are reasonably away from the rock boundary to avoid any boundary effects on crack propagation. The final fracture contour (i.e. fracture geometry at the end of the simulation) is shown in Fig. 10 which shows the different orientations of the final fracture geometry. When compared with the initial fracture geometry (Fig. 9), it can be observed that the shape of the fractures is changed to a bowl-like shape (Fig. 10).

The fracture propagation contour is compared with the existing literature (Castonguay et al., 2013) and is shown in Fig. 11 where the normalization is done against the initial fracture diameter d. Castonguay and his group modeled the hydraulic fracture propagation with symmetric Galerkin boundary element method (Castonguay et al., 2013). This method is based on the weak-form integral equation and allows to obtain the fracture data as a function of the position of fracture front. As can be observed from the Fig. 11, the fracture contour predicted in the current work matched well with that of the available

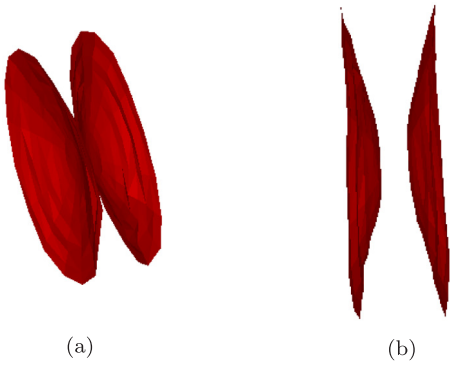

Fig. 10. Final geometry of two fractures in different orientations.

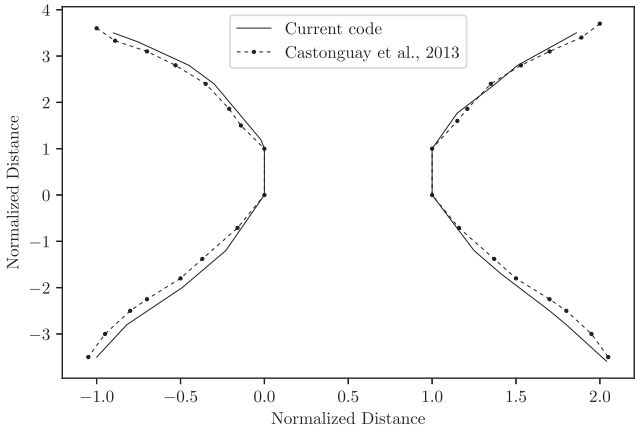

Fig. 11. The comparison of fracture propagation paths for two fractures.

literature (Castonguay et al., 2013). For generalizing the results, the normalized distance ($\frac{d_1}{d}$) is considered while plotting where d_1 is distance from center of wellbore, d is initial fracture diameter. In the current example, the simulation of the two fracture is modeled. In the next example, three simultaneous fracture propagations is simulated.

5.2. Three parallel fractures

In this example, the fracture propagation and interaction of three initially parallel fractures is observed for constant fluid flow rate (as shown in Fig. 12). This example is similar to the previous one, but a crack is added at the center. The boundaries of the rock sample are infinitely far from the wellbore. The material properties, dimensions and flow input parameters considered are given in Table 2 (after Castonguay et al., 2013).

After fluid injection, the fractures start propagating radially and each fracture is influencing the other fracture due to stress shadow effect. As the fracture becomes larger, the stress shadow effect also increases (Castonguay et al., 2013; Wu and Olson, 2015). The interaction and influence between the fractures also increases and the fractures start propagating away from each other. Due to combined stress shadow effect from both outer fractures, the central fracture will propagate only in the radial direction. The two outer fractures produce bowl-like contour. The initial fracture geometry is shown in Fig. 13.

The final fracture contour (i.e. fracture geometry at the end of the simulation) is shown in Fig. 14 in which the different orientations of the final fracture geometry can be observed. The normalization is again done against the initial fracture diameter d. When compared with the initial fracture geometry (Fig. 13), it can be observed that the shape of the outer fractures is changed to bowl shape and the fracture geometry is increased in radial direction.

The final fracture propagation contour is compared with the existing literature (Castonguay et al., 2013), in Fig. 15. As can be observed from

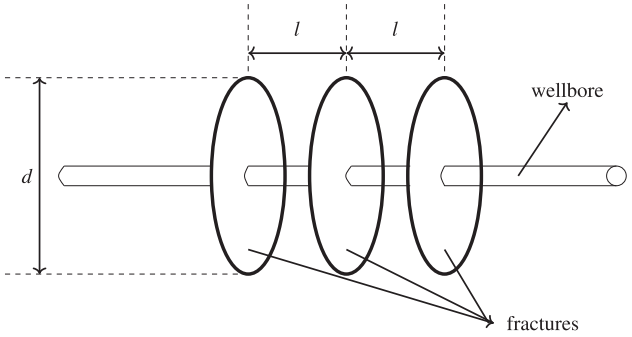

Fig. 12. A wellbore intersected by three parallel fractures.

Table 2
Input parameters for three parallel fractures.

Input parameters	Value
Flow rate (kg/s)	10
Poisson's ratio	0.25
Elastic modulus (GPa)	30
Rock Porosity	0.1
Permeability (m^2/s)	10^{-12}
Diameter of the fractures (m), d	5
Distance between fracture (m), l	5

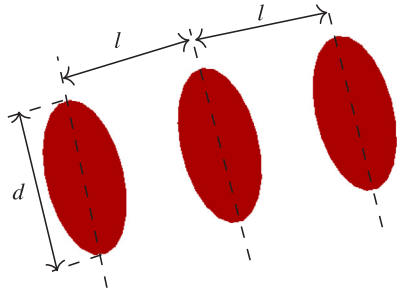

Fig. 13. Initial geometry of three fractures without wellbore.

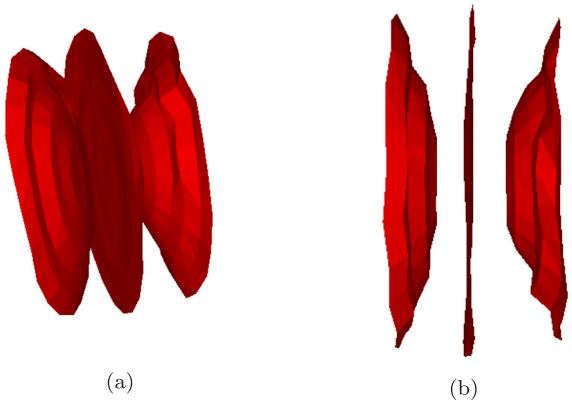

Fig. 14. Final geometry of three fractures in different orientations.

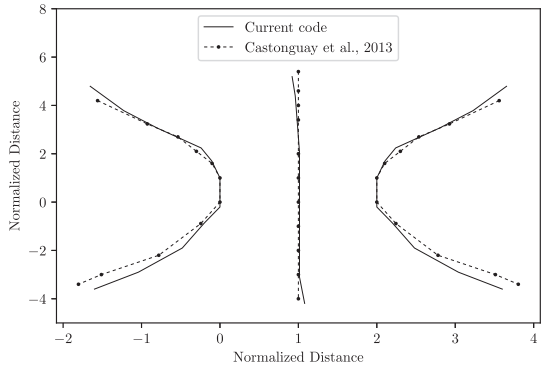

Fig. 15. The comparison of fracture propagation paths for three fractures.

the Fig. 15, the contour predicted in the current work matches well with that of the earlier work (Castonguay et al., 2013). For generalizing, normalized distance ($\frac{d_1}{d}$) is considered while plotting, where d_1 is distance from the center of wellbore and d is initial fracture diameter.

In this section, simulation of two and three fractures is modeled and validated. In the next section, the effect of initial fracture orientation on hydraulic fracture propagation is evaluated.

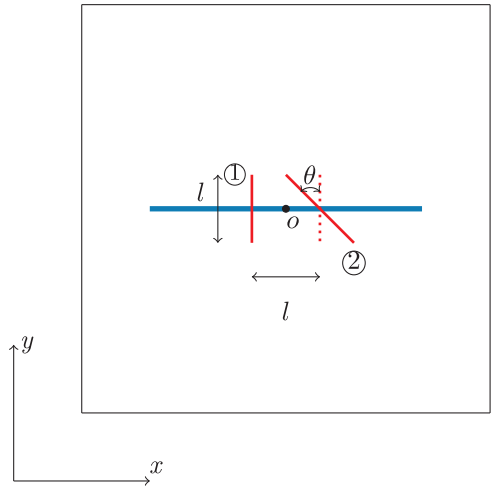

Fig. 16. A wellbore (blue line) intersected by two fractures (red lines). (For interpretation of the references to colour in this figure legend, the reader is referred to the web version of this article.)

6. Effect of initial fracture orientation on fracture propagation

Understanding the fracture propagation behavior is vital for optimizing the hydraulic fracture design. There are many factors such as fracture length (Su et al., 2015), orientation (Castonguay et al., 2013), viscosity of fluid (Zhou and Burbey, 2014), etc. which will effect the fracture propagation behavior. In this section, the effect of initial fracture orientation on the fracture propagation behavior is studied, which will influence the stress distribution in vicinity of fracture and changes the fracture propagation path. Understanding the influence of initial fracture orientation on fracture propagation is vital in hydraulic fracture design. Here, a wellbore with one fracture inclined with respect to the other is considered (as shown in Fig. 16). The geometry, material properties and loading conditions that are considered are given in Table 3 (after Wu and Olson, 2015).

Fig. 16 shows two fractures numbered ①and ②, with the latter at an inclination of θ. A total of six orientations (θ = 0°, 5°, 10°, 15°, 30°, 45°) are considered for fracture ②and fracture propagation behavior is studied. When fractures ①and ②are parallel to each other (θ = 0°), due to stress shadow effect, the fractures will propagate away from each other, similar to the behavior observed in Wu and Olson (2015). With increasing orientation angle θ, the fracture ②starts moving towards fracture ①. When the orientation angle θ reaches 15°, fracture ②intersects fracture ①. The results of fracture propagation are shown in Fig. 17.

For generalizing, the normalized distance ($\frac{d_2}{l}$) is considered while plotting, where d_2 is the distance from the center of wellbore o (as shown in Fig. 16), l is initial fracture diameter. Different fracture contours for various orientation angles θ are shown in Fig. 18. During hydraulic fracturing, improper initial fracture orientations will cause problems like incomplete drainage and poor areal sweep (Lacy, 1987). So, the fracture connectivity is very crucial for extracting shale gas in

Table 3
Input parameters for two parallel fractures.

Input parameters	Value
Flow rate (kg/s)	105
Poisson's ratio	0.35
Modulus elasticity (GPa)	30
Rock porosity	0.06
Permeability (m^2/s)	10^{-12}
Length of the fractures (m), l	10
Distance between fracture (m), l	10

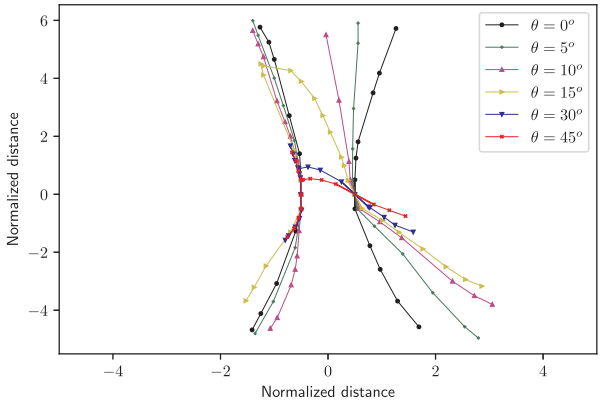

Fig. 17. The comparison of propagation paths for fractures with different initial orientations.

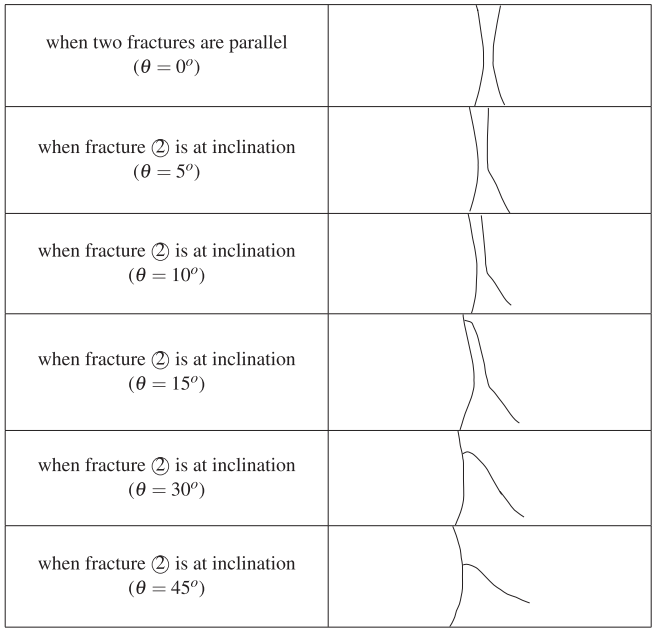

Fig. 18. The propagation paths of fractures with different initial orientations.

large quantities (Weng et al., 2011). As has been observed, different initial fracture orientations result in distinct fracture propagation patterns. Predicting the fracture pattern before doing actual hydraulic fracturing process in field will help in predicting output. Engineers can optimize the hydraulic fracture process and improve the overall economy of the procedure. In the current work, rock is assumed to follow elastic behavior and the fractures are allowed to propagate up to intersection. In other processes, like rock blasting, finding fragment size is crucial for optimizing the overall post-blast process (Cho et al., 2003). The initial fracture orientation producing different fracture propagation patterns (Fig. 18) will result in different fragment size distributions. The proposed method can predict the fracture propagation pattern for a particular fracture network in a rock.

7. Conclusion

In the present work, the TOUGH-FEMM simulator is used to investigate the interacting of two multiple hydraulic fractures in 3D. The rock is considered as linear elastic and mixed mode stress intensity factors are used for calculating fracture condition and propagation direction. The DCM is used for calculating stress intensity factors K_I, K_{II} and K_{III}.

The robustness and accuracy of the proposed simulation technique is demonstrated by solving and validating the three-dimensional hydraulic fracture problems with the existing literature. Using the TOUGH-FEMM simulator, the influence of initial fracture orientation on fracture propagation has been studied and it is observed that it has a significant effect on the final fracture geometry. When the fractures are initially parallel, owing to the stress shadow effect, the fractures propagate away from each other. As the initial fracture orientation increases (from 0° to 45°), the fractures tend to intersect with each other. The variation in the fracture propagation angle produces different fracture contours and different fragment shapes and sizes. It will have a significant effect on the shale gas/oil production. On the other hand, in blasting operations, the fragment shapes and sizes greatly affect the post-blast operations.

In the current work, fracture propagation up to intersection is considered, the extension of the proposed technique for simulating fracture coalescence will be pursued in the future. An experimental study may also be undertaken in the future to study the interaction and coalescence of fractures.

Acknowledgement

XT thanks the National Natural Science Foundation of China No. 41602296 and the National Key Research and Development Program of China No. 2017YFC1501300. GS thanks the Ministry of Mines, Government of India for support via S & T project F. No. 14/22/2015-Met IV.

References

Anderson, T., 2005. Fracture Mechanics, Fundamentals and Applications. CRC, Boca Raton.
Belytschko, T., Lu, Y.Y., Gu, L., 1994. Element-free galerkin methods. Int. J. Numer. Meth. Eng. 37 (2), 229–256.
Castelletto, N., Hajibeygi, H., Tchelepi, H.A., 2017. Multiscale finite-element method for linear elastic geomechanics. J. Comput. Phys. 331, 337–356.
Castonguay, S.T., Mear, M.E., Dean, R.H., Schmidt, J.H., et al., 2013. Predictions of the growth of multiple interacting hydraulic fractures in three dimensions. In: SPE Annual Technical Conference and Exhibition. Society of Petroleum Engineers.
Cho, S.H., Nishi, M., Yamamoto, M., Kaneko, K., 2003. Fragment size distribution in blasting. Mater. Trans. 44 (5), 951–956.
Christianovich, S., Zheltov, Y.P., 1955. Formation of vertical fractures by means of a highly viscous fluid. In: 4th World Petroleum Congress. vol. 2. pp. 579–586.
Fisher, M.K., Warpinski, N.R., et al., 2012. Hydraulic-fracture-height growth: real data. SPE Production & Operations 27 (1), 8–19.
Gupta, P., Duarte, C.A., 2016. Coupled formulation and algorithms for the simulation of non-planar three-dimensional hydraulic fractures using the generalized finite element method. Int. J. Numer. Anal. Meth. Geomech. 40 (10), 1402–1437.
He, Q., Suorineni, F., Oh, J., 2016. Review of hydraulic fracturing for preconditioning in cave mining. Rock Mech. Rock Eng. 49 (12), 4893–4910.
He, Q., Suorineni, F.T., Ma, T., Oh, J., 2017. Effect of discontinuity stress shadows on hydraulic fracture re-orientation. Int. J. Rock Mech. Min. Sci. 91, 179–194.
Hou, B., Zheng, C., Chen, D., Fan, M., Chen, M., 2016. Prediction of wellbore stability in conglomerate formation using discrete element method. Arab. J. Sci. Eng. 42, 4.
Ishida, T., 2001. Acoustic emission monitoring of hydraulic fracturing in laboratory and field. Constr. Build. Mater. 15 (5-6), 283–295.
Jung, Y., Pau, G.S.H., Finsterle, S., Pollyea, R.M., 2017. Tough3: a new efficient version of the tough suite of multiphase flow and transport simulators. Comput. Geosci. 108, 2–7.
Katsaga, T., Riahi, A., DeGagne, D., Valley, B., Damjanac, B., 2015. Hydraulic fracturing operations in mining: conceptual approach and DFN modeling example. Min. Technol. 124 (4), 255–266.
Kim, J., Moridis, G.J., 2013. Development of the t+ m coupled flow–geomechanical simulator to describe fracture propagation and coupled flow–thermal–geomechanical processes in tight/shale gas systems. Comput. Geosc. 60, 184–198.
Lacy, L., et al., 1987. Comparison of hydraulic-fracture orientation techniques. SPE Formation Evaluation 2 (01), 66–76.
Lancaster, P., Salkauskas, K., 1986. Curve and Surface Fitting: An Introduction. Academic Press.
Liu, Q., Sun, L., Tang, X., Chen, L., 2018. Simulate intersecting 3d hydraulic cracks using a hybrid 'fe-meshfree' method. Eng. Anal. Boundary Elem. 91, 24–43.
Lu, C., Li, M., Guo, J., Tang, X., Zhu, H., Wang, Y., H, L., 2015. Engineering geological characteristics and hydraulic fracture propagation mechanism of sand-shale interbedded formation in xu5 reservoir. J. Geophys. Eng. 12, 3.
Mei, J., Ni, Y., Li, J., 2011. The effect of crack orientation on fracture behavior of tantalum by multiscale simulation. Int. J. Solids Struct. 48 (21), 3054–3062.
Melenk, J.M., Babuška, I., 1996. The partition of unity finite element method: basic theory and applications. Comput. Methods Appl. Mech. Eng. 139 (1-4), 289–314.

Melin, S., 1983. Why do cracks avoid each other? Int. J. Fract. 23 (1), 37–45.
Minnebo, H., Majérus, J., Noels, L., 2010. Displacement extrapolation method: an alternative to j-integral for stress intensity factors computation using x-fem. In: Proceedings of IV European Conference on Computational Mechanics.
Moës, N., Dolbow, J., Belytschko, T., 1999. A finite element method for crack growth without remeshing. Int. J. Numer. Meth. Eng. 46 (1), 131–150.
Nakamura, T., Parks, D., 1988. Three-dimensional stress field near the crack front of a thin elastic plate. J Appl Mech 55, 805–813.
Nakamura, T., Parks, D., 1989. Antisymmetrical 3-d stress field near the crack front of a thin elastic plate. Int J Solids Struct 25 (12), 1411–1426.
Nejati, M., Paluszny, A., Zimmerman, R.W., 2015. On the use of quarter-point tetrahedral finite elements in linear elastic fracture mechanics. Eng. Fract. Mech. 144, 194–221.
Osiptsov, A.A., 2017. Fluid mechanics of hydraulic fracturing: a review. J. Petrol. Sci. Eng. 156, 513–535.
Paluszny, A., Zimmerman, R., 2013. Numerical simulation of multiple 3d fracture propagation using arbitrary meshes. Comput. Methods Appl. Mech. Eng. 200 (9-12), 953–966.
Perkins, T., Kern, L., et al., 1961. Widths of hydraulic fractures. J. Petrol. Technol. 13 (09), 937–949.
Pruess, K., Oldenburg, C., Moridis, G., 1999. Tough2 user's guide version 2. Tech. rep., Ernest Orlando Lawrence Berkeley National Laboratory, Berkeley, CA (US).
Rajendran, S., Zhang, B., 2007. A fe-meshfree quad4 element based on partition of unity. Comput. Methods Appl. Mech. Eng. 197 (1-4), 128–147.
Rinaldi, A.P., Nespoli, M., 2017. Tough2-seed: a coupled fluid flow and mechanical-stochastic approach to model injection-induced seismicity. Comput. Geosci. 108, 86–97.
Rinaldi, A.P., Rutqvist, J., 2017. Modeling ground surface uplift during CO_2 sequestration: the case of in salah, algeria. Energy Procedia 114, 3247–3256.
Rutqvist, J., 2011. Status of the tough-flac simulator and recent applications related to coupled fluid flow and crustal deformations. Comput. Geosci. 37 (6), 739–750.
Rutqvist, J., 2017. An overview of tough-based geomechanics models. Comput. Geosci. 108, 56–63.
Rutqvist, J., Stephansson, O., 2003. The role of hydromechanical coupling in fractured rock engineering. Hydrogeol. J. 11 (1), 7–40.
Shimizu, H., Ito, T., Tamagawa, T., Tezuka, K., 2018. A study of the effect of brittleness on hydraulic fracture complexity using a flow-coupled discrete element method. J. Petrol. Sci. Eng. 160, 372–383.
Sih, G.C., 1974. Strain-energy-density factor applied to mixed mode crack problems. Int. J. Fract. 10 (3), 305–321.
Strifors, H.C., 1974. A generalized force measure of conditions at crack tips. Int. J. Solids Struct. 10 (12), 1389–1404.
Su, Y., Ren, L., Meng, F., Xu, C., Wang, W., 2015. Theoretical analysis of the mechanism of fracture network propagation with stimulated reservoir volume (SRV) fracturing in tight oil reservoirs. PloS one 10 (5), 1–25.
Sukumar, N., Moës, N., Moran, B., Belytschko, T., 2000. Extended finite element method for three-dimensional crack modelling. Int. J. Numer. Meth. Eng. 48 (11), 1549–1570.
Taleghani, A.D., Gonzalez-Chavez, M., Yu, H., Asala, H., 2018. Numerical simulation of hydraulic fracture propagation in naturally fractured formations using the cohesive zone model. J. Petrol. Sci. Eng. 165, 42–57.
Tang, X., Rutqvist, J., Hu, M., Rayudu, N., in preparation. Modeling three-dimensional fluid-driven propagation of multiple fractures using tough-femm. Rock Mech. Rock Eng.
Tang, X., Zheng, C., Wu, S., Zhang, J., 2009. A novel virtual node method for polygonal elements. Appl. Math. Mech. 30 (10), 1233–1246.
Weng, X., Kresse, O., Cohen, C.E., Wu, R., Gu, H., et al., 2011. Modeling of hydraulic fracture network propagation in a naturally fractured formation. In: SPE Hydraulic Fracturing Technology Conference. Society of Petroleum Engineers.
Wu, K., Olson, J., 2013. Simultaneous multifracture treatments: fully coupled fluid flow and fracture mechanics for horizontal wells. SPE Annual Technical Conference and Exhibition, New Orleans.
Wu, K., Olson, J.E., et al., 2015. Simultaneous multifracture treatments: fully coupled fluid flow and fracture mechanics for horizontal wells. SPE J. 20 (02), 337–346.
Wu, R., Kresse, O., Weng, X., Cohen, C., Gu, H., 2012. Modeling of interaction of hydraulic fractures in complex fracture networks. SPE Hydraulic Fracturing Technology Conference, 6–8 February, The Woodlands, Texas, USA 1, 1.
Yan, C., Zheng, H., Sun, G., Ge, X., 2016. Combined finite-discrete element method for simulation of hydraulic fracturing. Rock Mech. Rock Eng. 49 (4), 1389–1410.
Yang, Y., Chen, L., Tang, X., Zheng, H., Liu, Q., 2017. A partition-of-unity based 'fe-meshfree' hexahedral element with continuous nodal stress. Comput. Struct. 178, 17–28.
Yang, Y., Tang, XH, Zheng, H., Liu, Q., Liu, Z., 2018. Hydraulic fracturing modelling using the enriched numerical manifold method. Appl. Math. Model. 53, 462–486.
Yang, Y., Tang, X., Zheng, H., 2014. A three-node triangular element with continuous nodal stress. Comput. Struct. 141, 46–58.
Yang, Y., Tang, X., Zheng, H., Liu, Q., He, L., 2016. Three-dimensional fracture propagation with numerical manifold method. Eng. Anal. Boundary Element Method 72, 65–77.
Zhai, C., Li, M., Sun, C., Zhang, J., Yang, W., Li, Q., 2012. Guiding-controlling technology of coal seam hydraulic fracturing fractures extension. Int. J. Min. Sci. Technol. 22 (6), 831–836.
Zhao, Z., Guo, J., Ma, S., 2015. The experimental investigation of hydraulic fracture propagation characteristics in glutenite formation. Adv. Mater. Sci. Eng. 2015.
Zhou, X., Burbey, T.J., 2014. Fluid effect on hydraulic fracture propagation behavior: a comparison between water and supercritical CO_2-like fluid. Geofluids 14 (2), 174–188.